Optica Applicata, Vol. XLIII, No. 4, 2013
DOI: 10.5277/oa130409

A method for probing the refractive index change in photorefractive crystals

MIN FU[1], CHENGYONG GAO[1*], XU'AN WANG[2], YUANKAI CUI[1], SHUWEI DAI[1]

[1]School of Physics, Shandong University, Jinan 250100, China

[2]Department of Physics and Electronics, Binzhou College, Binzhou 256600, China

[*]Corresponding author: happyfumin@gmail.com, gchy@sdu.edu.cn

A method for probing refractive index changes in photorefractive crystals using an interferometric technique and digital image processing was proposed. Based on equal thickness interference in $LiNbO_3$ crystal and Fourier transform profilometry, we obtained phase value changes in interferograms induced by a photorefractive effect, and further calculated refractive index changes. The maximal values for extraordinary light (e-light) and ordinary light (o-light) are 6.6×10^{-4} and 1.2×10^{-4}, respectively.

Keywords: Fourier transform profilometry, refractive index change, photorefractive effect.

1. Introduction

Interferometric method is an effective way to measure the refractive index changes in photorefractive crystals [1]. BLISS *et al*. [2] used Mach–Zehnder interferometer to observe the variation of the refractive index with intensity in laser materials. MILAN and WEBER [3] and OLBRIGHT and PEYGHAMBARIAN [4] employed Michelson interferometer and Twyman–Green interferometer to measure the nonlinear index of refraction respectively. However, interferometer accuracy is limited by interference fringe counting. Hardware and software fringe counting are two major ways used to record the number of fringes [5]. For hardware fringe counting, trigger circuit converts interference signals into square waves, then a reversible counter is activated by the square waves to add or subtract counts. The main disadvantage of hardware fringe counting is that the electronically countable shift of $\pi/2$ corresponds to the phase shift of $\pi/8$, which is the resolution limit for existing hardware fringe counting. For software fringe counting, the image is processed and counted based on gray-level morphology. But its accuracy is limited by the variations of intensity and spacing of the fringes.

In this paper, we proposed an approach to measure the refractive index changes in photorefractive crystals by integrating a traditional interferometric technique and Fourier

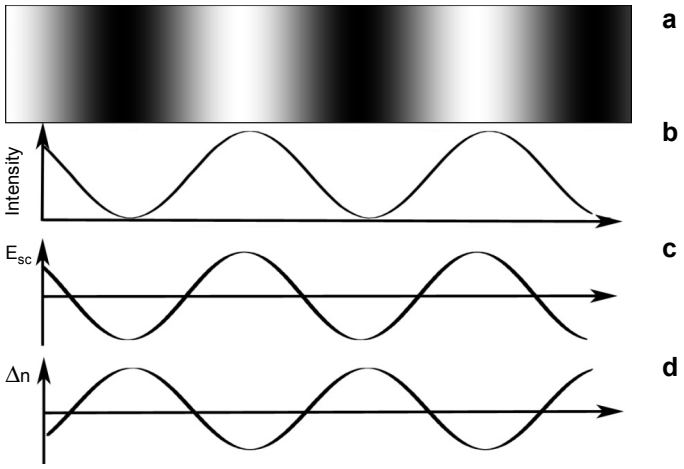

Fig. 1. Simulation of refractive index changes in the sample (see text for explanation).

transform profilometry (FTP). It has several advantages. First, only one (or two) fringe(s) is needed, which makes real-time and dynamic data processing possible [6]; second, FTP is a global transform method, which makes it more tolerant to noises [7].

The light used in the interferometric method is a collimated beam, because it seems that uniform light illumination is not suitable to induce photorefractive (PR) effect in the sample. However, it is the light intensity changes in the interferogram that introduce PR effect. Figure 1 depicts this process: when illuminated by non-uniform light (Fig. 1**a**), charge carriers are excited in the sample for the non-uniform light intensity (Fig. 1**b**) of the interferometric fringes [8]. Under the influence of a strong photovoltaic (PV) effect in $LiNbO_3$ (LN) crystal, the charge carriers drift in the crystal and are then trapped. As a result, a spatial charge distribution (Fig. 1**c**) is set up. Space charge field E_{sc} is along *c*-axis in the illuminated area and changes its sign at the edge of the illuminated strip by means of an electro-optic effect (Pockels effect). This field creates refractive changes (Fig. 1**d**) in LN crystal, which can be expressed as

$$\Delta n_i = -n_i^3 \gamma_{\text{eff}} \frac{E_{\text{sc}}}{2}, \qquad i = o, e \tag{1}$$

where γ_{eff} are the efficient electro-optic coefficients. When the light polarization is vertical to *c* axis, $\Delta n_o = -n_o^3 \gamma_{13} E_{\text{sc}}/2$. When the light polarization is along axis *c*, $\Delta n_e = -n_e^3 \gamma_{33} E_{\text{sc}}/2$. For LN crystal $\gamma_{13} = 8.6\times10^{-12}$ m/V and $\gamma_{33} = 30.8\times10^{-12}$ m/V, therefore the refractive index changes for e-light are greater than o-light.

2. Experiment

The experiment setup based on the Michelson interference principle is shown in Fig. 2. The light source is a 532 nm semiconductor laser with the incident intensity of 3.5 mW and the laser beam is collimated in our case. The sample (pure $LiNbO_3$ crystal,

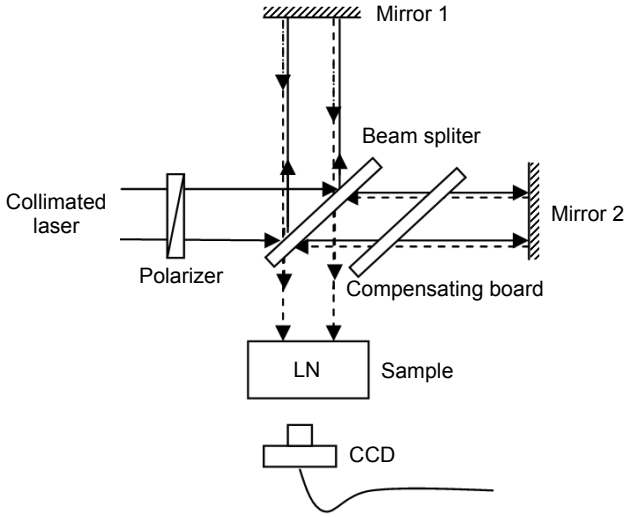

Fig. 2. Experiment setup.

the size is 9.4×4.5×2.87 mm^3 cut along *a*, *b* and *c* crystallographic axis) is placed at the end of the optical path. A polarizer plate is placed into the optical path, whose polarization direction is vertical or parallel to the optical axis of the sample. We project the interferograms on a glass screen with rectangular coordinates on it and adjust the two plane mirrors to get vertical equal thickness interferograms without the existence of the crystal; the interferograms are recorded by CCD after the crystal is put in the light path.

Figure 3 shows the displacement of fringe patterns under e-light at the time of 30, 35, 40, and 45 s. Refractive index changes in PR crystal can be calculated by analyzing the interferogram formed in it; the method is further explained in the next part. The fringe pattern changes for o-light are similar to e-light, only its changes are slower.

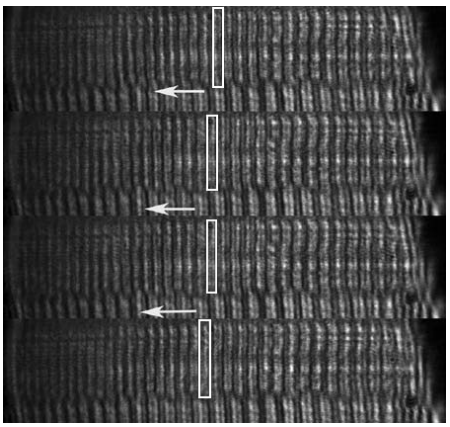

Fig. 3. Displacement of fringe patterns under e-light at the time of 30, 35, 40, 45 s from top to bottom.

3. Experimental data analysis

TAKEDA and MUTOH [9] described the Fourier transform method for the fringe pattern analysis and suggested that the carrier phase component could be removed in the frequency domain via a spectrum shift.

The interferogram can be interpreted as a deformed fringe pattern, which can generally be expressed as:

$$I = I_O + I_M\left(2\pi\omega_c + \varphi\right) \tag{2}$$

where I, I_O and I_M are the recorded intensity, background intensity and modulation intensity, respectively; ω_c is the frequency of the carrier fringe; and φ is the phase angle [10]. It can also be written as:

$$I = I_O + \frac{1}{2}I_M\exp\left(2\pi j\omega_c + j\varphi\right) + \frac{1}{2}I_M\exp\left(-2\pi j\omega_c - j\varphi\right) =$$
$$= I_O + I_e + I_e^* \tag{3}$$

where $j = \sqrt{-1}$, I_e and I_e^* are complex conjugates. Since the carrier frequency is introduced, the three spectra are separated in the frequency domain. By applying the Fourier transform and spectrum shift to remove the carrier, phase data can be extracted from the fringe pattern. After the inverse Fourier transform, a wrapped phase map can be obtained with the carrier phase component removed. A phase unwrapping process could subsequently retrieve continuous phase distributions.

Because the influence of refractive index changes on all fringes is homogeneous, we choose the area with bright uniform illumination in image processing. Figure 4**b** shows the target area cropped from the original interferogram, both 256 pixels large.

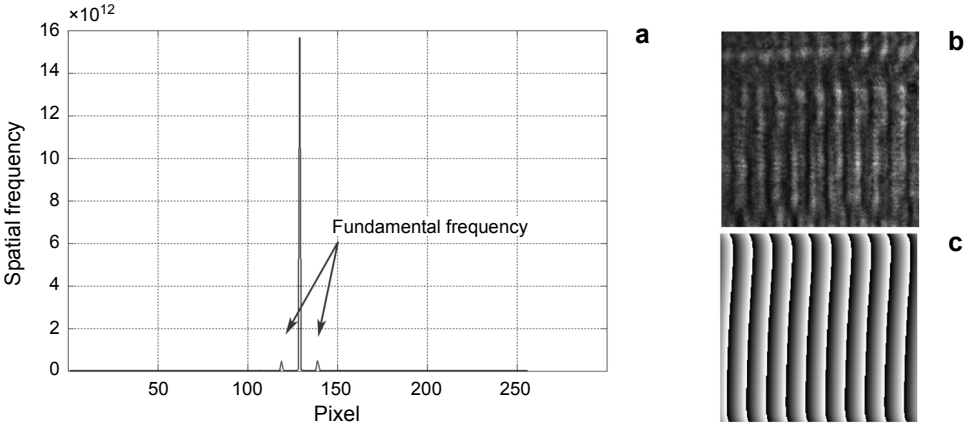

Fig. 4. Spatial frequency spectra (**a**), target interferogram (**b**), and wrapped phase distribution (**c**).

The digital matrix of this area is first processed by a 3×3 median filter to lower the noise. Frequency domain is obtained by applying a 2-dimensional FFT (fast Fourier transform) algorithm. For clarity and convenience in graphic presentation, Fig. 4**a** shows only the frequency domain information of the 129th row of the processed area, *x*-coordinate represents the pixel in columns. This also explained Fig. 4**a**'s similarity to a 1-dimensional Fourier transform frequency domain. The positive fundamental frequency is moved to the center of the frequency spectrum to erase the carrier phase. Figure 4**c** indicates the phase distribution without the carrier phase component produced by a two-dimensional inverse Fourier transform of the shifted spectrum.

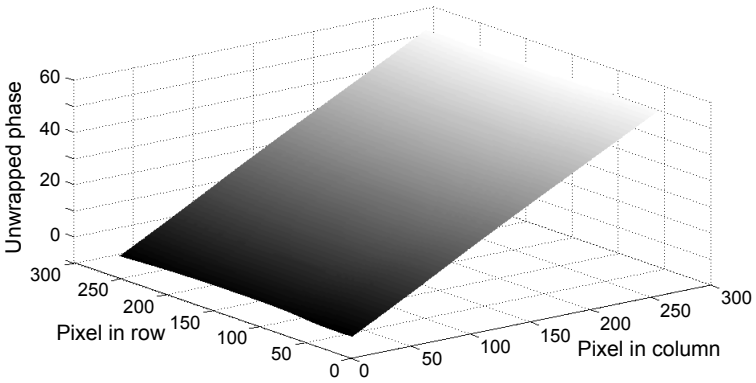

Fig. 5. Unwrapped phase distribution at t = 45 s, under e-light.

All the phase values obtained are in the range of $-\pi$ to π. Therefore phase unwrapping is needed to remove the 2π discontinuity to generate a smooth phase map. Figure 5 shows the unwrapped phase map at t = 45 s, when the light polarization is along *c*-axis. The average phase value of the 256th column can be interpreted as the phase value of the corresponding interferogram at different time. The phase value difference between two adjacent times is calculated by

$$\Delta\varphi = \begin{cases} \varphi_c - \varphi_p, & \varphi_c > \varphi_p \\ \varphi_c - \varphi_p + 2\pi, & \varphi_c < \varphi_p \end{cases} \tag{4}$$

where φ_c is the phase value of current time, φ_p is the phase value of previous time. The relation of the phase change $\Delta\varphi$, optical path l, wavelength λ, refractive index change between two adjacent time Δn_i is:

$$\left|\Delta n_i\right| = \frac{\Delta\phi\,\lambda}{2\pi\, l}, \qquad i = o, e \tag{5}$$

The refractive index change at a given time is the integral of all preceding refractive index changes. We processed all collected interferograms this way and got the relation

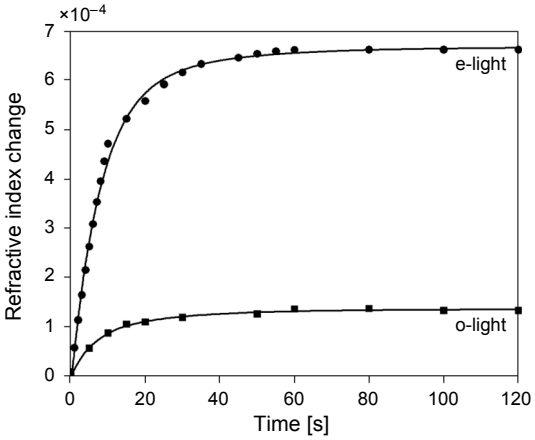

Fig. 6. Relation of refractive index change with increasing time.

of refractive index changes with increasing time in $LiNbO_3$ sample (Fig. 6). The interferograms and the corresponding phase values remain unchanged after $t = 60$ s, which means that refractive index changes reach a steady-state value in about 60 s of persisting illumination. Maximal refractive index modulation in the sample is 1.2×10^{-4} for o-light and 6.6×10^{-4} for e-light. The results coincide with the theoretical value and other research results [3–5].

4. Conclusions

In this research we applied the interferometric method to measure the refractive index changes in photorefractive crystals. The saturation refractive index changes in LN sample under a 3.5 mW, 532 nm laser are 1.2×10^{-4} for o-light and 6.6×10^{-4} for e-light. Although the use of the Michelson interferometer to measure the refractive index changes in crystals is common, the proposed method adopts FTP in image processing to decrease the inaccuracy in fringe counting. This modified interferometer technique achieves automatic, non-destructive, and convenient in refractive index variation measurement. This method can be used to investigate a refractive index change as a function of temperature, wavelength, light intensity *etc*. in light-sensitive materials as well as to determine the nonlinear refractive-index coefficients in PR materials.

Acknowledgements – The authors are thankful to Innovation Fund of Shandong University, China (Grant No. 2010TS017).

References

[1] ZHANG J., XU J.Q., GAO C.Y., SI S.C., *Modified Michelson interferometer for probing refractive index of birefringent crystal CSBN50*, Optics and Lasers in Engineering **47**(11), 2009, pp. 1212–1215 .

[2] BLISS E.S., SPECK D.R., SIMMONS W.W., *Direct interferometric measurements of the nonlinear refractive index coefficient n_2 in laser materials*, Applied Physics Letters **25**(12), 1974, pp. 728–730.

[3] MILAM D., WEBER M.J., *Measurement of nonlinear refractive-index coefficients using time-resolved interferometry: Application to optical materials for high-power neodymium lasers*, Journal of Applied Physics **47**(6), 1976, pp. 2497–2501.

[4] OLBRIGHT G.R., PEYGHAMBARIAN N., *Interferometric measurement of the nonlinear index of refraction, n_2, of CdS_xSe_{1-x}-doped glasses*, Applied Physics Letters **48**(18), 1986, pp. 1184–1186.

[5] BENYONG CHEN, JIANBO LUO, DACHENG LI, *Code counting of optical fringes: methodology and realization*, Applied Optics **44**(2), 2005, pp. 217–223.

[6] XIANYU SU, WENJING CHEN, *Fourier transform profilometry: a review*, Optics and Lasers in Engineering **35**(5), 2001, pp. 263–284.

[7] QIAN KEMAO, *Windowed Fourier transform for fringe pattern analysis*, Applied Optics **43**(13), 2004, pp. 2695–2702.

[8] KÖSTERS M., BECHER C., HAERTLE D., STURMAN B., BUSE K., *Charge transport properties of undoped congruent lithium niobate crystals*, Applied Physics B **97**(4), 2009, pp. 811–815.

[9] TAKEDA M., MUTOH K., *Fourier transform profilometry for the automatic measurement of 3-D object shapes*, Applied Optics **22**(24), 1983, pp. 3977–3982.

[10] C. QUAN, C.J. TAY, L.J. CHEN, *A study on carrier-removal techniques in fringe projection profilometry*, Optics & Laser Technology **39**(6), 2007, pp. 1155–1161.

Received March 27, 2013
in revised form May 12, 2013